processes

MDPI

Article

Multiphase Semi-Empirical Productivity Evaluation Method of Shale Reservoir Based on Production Performance and Flow Mechanism

Rui Wang [1,2,3,*] and He Liu [1,2,4]

[1] College of Petroleum Engineering, Northeast Petroleum University, Daqing 163000, China; liuhe@petrochina.com.cn
[2] State Key Laboratory of Continental Shale Oil (SKL-CSO), Daqing 163712, China
[3] PetroChina Daqing Oilfield Co., Ltd., Daqing 163712, China
[4] PetroChina Research Institute of Petroleum Exploration & Development, Beijing 100083, China
* Correspondence: wr20260313@163.com

Abstract

The complex fracture networks, multiphase flow behavior, and nonlinear flow mechanisms induced by hydraulic fracturing in horizontal wells of shale oil reservoirs pose significant challenges to production evaluation. In this study, a semi-empirical productivity evaluation method for multiphase shale oil systems is developed by integrating production dynamics with flow mechanisms. Three-phase productivity equations for oil, gas, and water are established, explicitly incorporating the underlying flow mechanisms. A nonlinear flow index is introduced to characterize both the stress sensitivity of fractures and the threshold pressure gradient in the matrix. Key unknown parameters, including oil saturation, water cut, stimulated reservoir volume, and nonlinear coefficients, are determined through history matching of production data. The impacts of geological properties, fracturing parameters, operating conditions, and nonlinear flow parameters on oil–gas productivity are systematically investigated using the proposed multiphase semi-empirical model. The model is validated against production data from fractured horizontal wells in a field case, demonstrating its accuracy and applicability. Furthermore, the model enables reliable production forecasting based on the derived productivity relationships. The proposed approach provides a practical and efficient tool for rapid post-fracturing productivity evaluation in shale oil reservoirs.

Keywords: shale oil reservoir; semi-empirical productivity evaluation; nonlinear flow mechanism; history matching; multiphase

Check for updates

Academic Editors: Wente Niu, Mingqiang Wei and Ying Mu

Received: 1 April 2026
Revised: 17 April 2026
Accepted: 21 April 2026
Published: 26 May 2026

Copyright: © 2026 by the authors. Licensee MDPI, Basel, Switzerland. This article is an open access article distributed under the terms and conditions of the Creative Commons Attribution (CC BY) license.

1. Introduction

Volume fracturing of horizontal wells has become the main development method for increasing the single-well production and ultimate recovery rate of shale oil and gas reservoirs. The complex fracture network formed after fracturing significantly alters the flow characteristics of the reservoir, causing shale oil reservoirs to exhibit multi-medium, multi-scale, and strongly nonlinear flow behaviors. Therefore, establishing a production capacity prediction model that can reasonably represent the structural and flow mechanism of the complex fracture network is of great significance for the efficient development of shale oil reservoirs. Currently, the models used to simulate the productivity of volume

fracturing horizontal wells can be mainly classified into three categories: decline analysis methods, analytical models, and numerical models.

The decline analysis methods include the Wattenbarger linear flow method [1], PLE power-exponential decline model method [2,3], SEPD extended exponential decline model method [4], Duong decline model method [5], LGM model method [6], continuous solution method [7], pseudo-steady-state pressure solution method [8], horizontal well multi-stage fracturing analytical model method [9–12], etc. The Wattenbarger linear flow method, pseudo-steady-state pressure solution method, and horizontal well multi-stage fracturing analytical model method can predict the single-well production under variable bottom-hole flow pressure. The Wattenbarger linear flow method is applicable to the pseudo-steady-state stage; the pseudo-steady-state pressure solution method and the horizontal well multi-stage fracturing analytical model method are applicable to linear flow, bilinear flow, and the pseudo-steady-state stage; but the horizontal well multi-stage fracturing analytical model method has stricter application requirements and requires the determination of the fracture network parameters after fracturing. The PLE method, SEPD method, Duong method, LGM method, and continuous solution method can solve the production analysis problem under stable bottom-hole pressure production. The SEPD method is applicable to the pseudo-steady-state stage, while the other four methods are applicable to linear flow, bilinear flow, and pseudo-steady-state stage. Currently, the decline analysis methods consider more complex fracture networks, but less on the flow mechanism.

The analytical models are usually based on the linear flow assumption. By dividing the fractured treatment area and its surrounding regions, the flow within different areas is simplified to linear flow or pseudo-steady-state flow, and the overall coupling is achieved through regional boundary conditions. Studies have shown that on the double-logarithmic plot of the typical production curve of shale gas and oil fracturing horizontal wells, obvious linear segment characteristics can often be observed. This phenomenon is considered to be the result of non-steady linear fluid flow from the low-permeability matrix to the fractures. Wattenbarger [13] was the first to propose the linear flow model, and, through the division of flow stages, gave the analytical expressions for the linear flow stage and the boundary control flow stage. On this basis, Al-Ahmadi et al. [14] introduced the spatial combination relationship between artificial fractures and natural fractures and established a triple-medium linear flow model, which more systematically described the zone flow process of the near-well area after fracturing. Tivayanonda [15] further simplified the artificial fractures to infinite conducting fractures and proposed several typical production curves to assist in the identification of flow stages. To overcome the shortcomings of the flat model in ignoring the influence of the external area of the fracturing treatment, Brown et al. [10] proposed the trilinear flow model, dividing the reservoir into the internal and external treatment areas of the fracturing; Brohi et al. [12], Xu et al. [16], and Stalgorova et al. [17] further expanded this model and systematically analyzed the contribution of the external area and inter-fault regions to the production in the middle and later stages. Due to the difficulty of the analytical models in depicting the complex fracture network structure, some scholars proposed semi-analytical methods based on point source functions. This type of method discretizes the artificial fractures of the fracturing horizontal well into multiple nodes, uses the superposition principle to construct the pressure and production coupling relationship between each node, and combines the boundary conditions to form a closed matrix for iterative solutions [18–21]. The analytical models simplify the complex flow process into multiple linear flow units by reasonable partitioning of the near-well area, and have the advantages of clear physical concepts and high computational efficiency. However, their description ability for complex fracture networks and nonlinear flow mechanisms is limited. The semi-analytical models achieve a certain balance between computational

efficiency and fracture description ability and are suitable for engineering analysis of multi-stage fracturing horizontal wells. However, their essence is still based on the linear flow theory and have limited ability to depict strong nonlinear flow mechanisms.

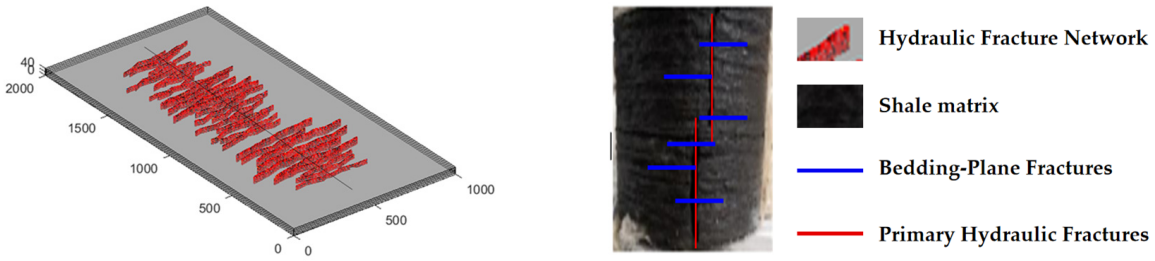
The numerical simulation method is also a common approach for dealing with complex fracture networks and nonlinear flow mechanisms. Discrete Fracture Models (DFM) and Embedded Discrete Fracture Models (EDFM) based on finite difference, finite volume, and finite element methods [22–24] have been widely applied in the field of numerical simulation of shale oil and gas reservoirs. However, these methods generally have problems such as complex numerical model establishment, high requirements for grid division fineness, and high computational costs [25,26]. The Green's element method, as a combination of boundary element method and finite element method, has high accuracy in handling heterogeneous and nonlinear problems [27], but its modeling and solution process is relatively complex, and its application in rapid engineering evaluation is still limited to a certain extent.

The decrement analysis method is highly practical but cannot take into account complex flow mechanisms. The analytical model is computationally efficient but has limited application scope. The numerical model has strong physical representation capabilities but has high computational costs. Therefore, within the analytical framework, more key flow mechanisms that are more in line with the actual conditions of shale oil reservoirs were introduced, and a multiphase semi-empirical productivity evaluation method considering the flow mechanisms of shale reservoirs was constructed.

2. Hydraulic Fracture Network and Production Characteristics

2.1. Characteristics of Fracture Networks in Shale Reservoirs

During the fracturing process of GuLong shale, the extension of the fracture network presents a clear directional expansion law: under the control of strong heterogeneity of the reservoir, hydraulic fractures first extend horizontally along the mechanical weak surface, that is, densely developed horizontal bedding and bedding fractures, forming the main fracture network plane, as shown in Figure 1a. Subsequently, driven by continuous high pressure, the cracks puncture vertically in the upward and downward directions, penetrate the brittle interlayer and communicate with multiple sets of laminae, and finally form a 'Feng'-shaped three-dimensional complex fracture network connected by transverse main fractures and three-dimensionally interwoven by vertical branch fractures, as shown in Figure 1b. This structure greatly increases the effective transformation volume, which is the key to realize the efficient utilization of shale reservoirs.



(**a**) Horizontal characteristics of fracture network (**b**) Vertical characteristics of fracture network

Figure 1. Characteristics of complex fracture network structure.

2.2. Three-Phase Multi-Stage Migration Process of Shale Reservoirs

The Gu Long shale oil reservoir is of light oil type. Its composition is shown in Table 1. The GuLong shale oil in the northern part of the Songliao Basin is typical continental shale oil. The lithology is mainly composed of mud shale with a particle size less than 3.9 μm.

The cumulative thickness of other lithologies such as siltstone and carbonate rock that are interbedded with the mud shale accounts for less than 10% of the total thickness, and it is a shale-type shale oil [28].

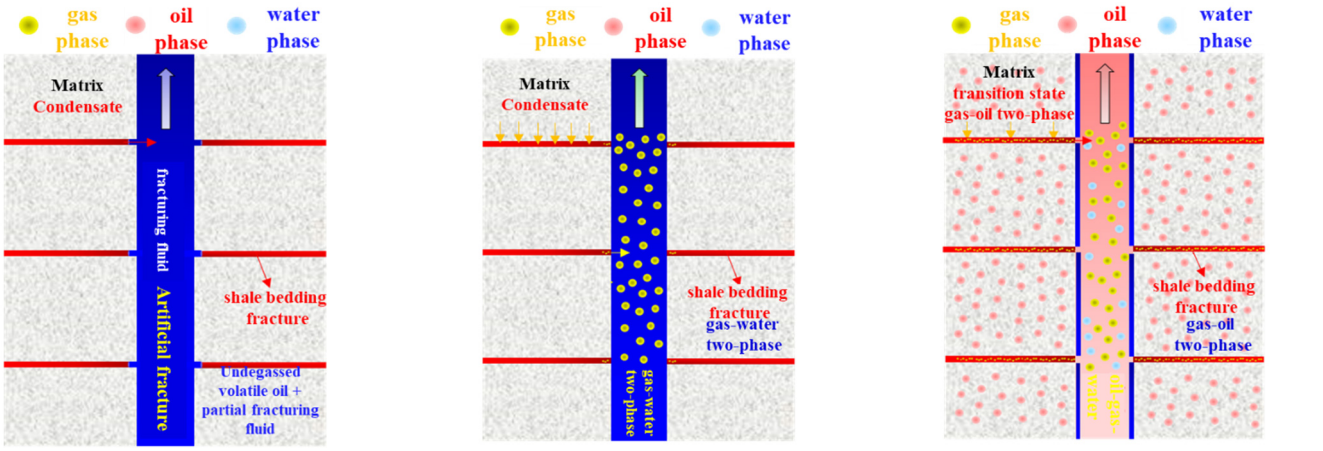
Table 1. Formation crude oil components.

Gas Composition	Mole Fraction (%)
N_2	1.8627
CO_2	3.9822
C1	54.8441
$C_{2–5}$	23.5505
$C_{6–10}$	4.5928
$C_{11–20}$	7.9004
$C_{21–30}$	3.2533

In the early stage of post-fracturing flowback of the GuLong shale, it is difficult for the fluid in the matrix system to flow effectively in a short period of time, and it is basically in an unused state. The natural bedding fracture system has a certain conductivity, which can not only produce some residual fracturing fluid, but also produce formation crude oil with imbibition displacement and pressure conduction, forming the characteristics of oil and water co-production. The newly formed artificial main fracture is mainly used as a fast flow channel of fracturing fluid in the early stage of flowback, and a large amount of fracturing fluid dominated by the water phase is preferentially discharged, showing obvious characteristics of single-phase water production.

In the early stage of depressurization mining of the GuLong shale reservoir, the light hydrocarbon components adsorbed in the matrix system first desorb and form a small amount of the free gas phase. The gas mainly migrates slowly through diffusion. The bedding fracture has relatively good conductivity and a large contact area with the matrix. Under the pressure drop transmission, the gas phase diffuses from the matrix and a small amount of the degassed gas phase that precipitated from the crude oil in the bedding fracture generates a differential pressure displacement power to displace a small amount of oil and gas into the connected artificial fracture. In the artificial main fracture, as the gas phase is gradually replenished from the matrix and the bedding fracture, the continuous gas phase begins to appear in the fracture, and the flow pattern gradually transitions from the initial water phase to the gas–water two-phase flow, showing obvious gas–water two-phase output characteristics.

In the middle stage of depressurization mining, as the formation pressure continues to decrease significantly, more complex multiphase flow dynamics are presented in the reservoir. A large amount of dissolved gas in the crude oil of the matrix system is precipitated to form a high gas saturation, resulting in a sharp decrease in the relative permeability of the oil phase. After degassing, the viscosity of the crude oil increases and the fluidity deteriorates, which makes the effective flow capacity of the oil and gas phases decrease significantly, and both the gas diffusion and oil phase flow enter the low-speed stage. The bedding fracture system has become an important transition and supply channel: the gas from the matrix continues to diffuse into the bedding fracture, and the crude oil is degassed to form a continuous gas phase flow, which forms a two-phase flow with a certain flow capacity with the oil phase. In the artificial main fracture, the early residual fracturing fluid water phase still exists, and the oil phase from the bedding fracture and the matrix continues to produce a supply, showing obvious oil–gas–water three-phase output characteristics. The three stages described above are shown in Figure 2.



(**a**) Initial stage of backflow

(**b**) Initial stage of depressurization mining

(**c**) Middle stage of depressurization mining

Figure 2. Characteristics of multiphase migration stage.

It is essential to clarify the applicability of the linear flow assumption within the context of shale oil production life cycles. Due to the ultra-low permeability of shale matrices, pressure disturbances propagate extremely slowly, typically keeping the system within the linear flow regime for decades. While fracture–matrix bilinear flow may be observed in early-time diagnostic plots, its duration is remarkably brief owing to high fracture conductivity, which allows the fractures to reach a steady-state rapidly. Crucially, the primary fluid transport mechanism from the matrix toward the fracture remains linear in both the bilinear and linear flow stages. Consequently, the boundary-dominated flow (BDF) is rarely encountered during the typical economic life of shale wells. Thus, the linear flow assumption serves as a robust and representative simplification that accurately captures the production dynamics of shale oil reservoirs throughout their entire development span.

3. Evaluation Formula of Multiphase Productivity

3.1. Water-Phase Semi-Empirical Productivity Evaluation Model Construction

The water phase mainly occurs in the fracture network formed by hydraulic fracturing in the reservoir. After the start of production, as the bottom-hole pressure decreases, the fracture system releases its stored elastic energy under the combined action of closure stress and internal fluid pressure. This elastic energy is converted into driving pressure, so that the water phase in the fracture flows to the wellbore along the fracture channel and is eventually discharged into the wellbore. This process is shown in Figure 3. This process is an important mechanism for the initial water production of the reservoir after fracturing, and also creates flow conditions for the subsequent flow of the oil phase and gas phase.

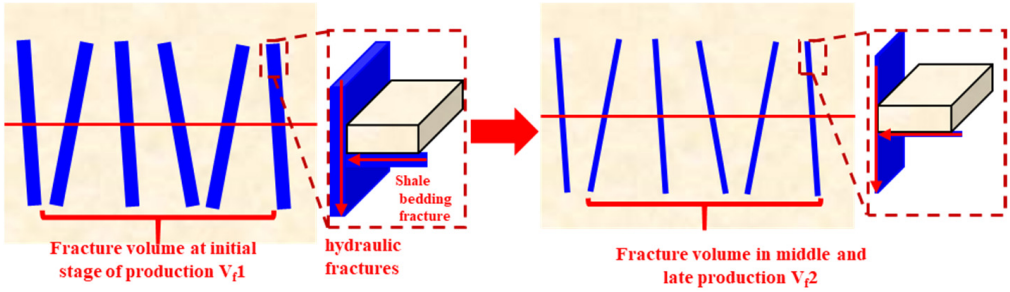
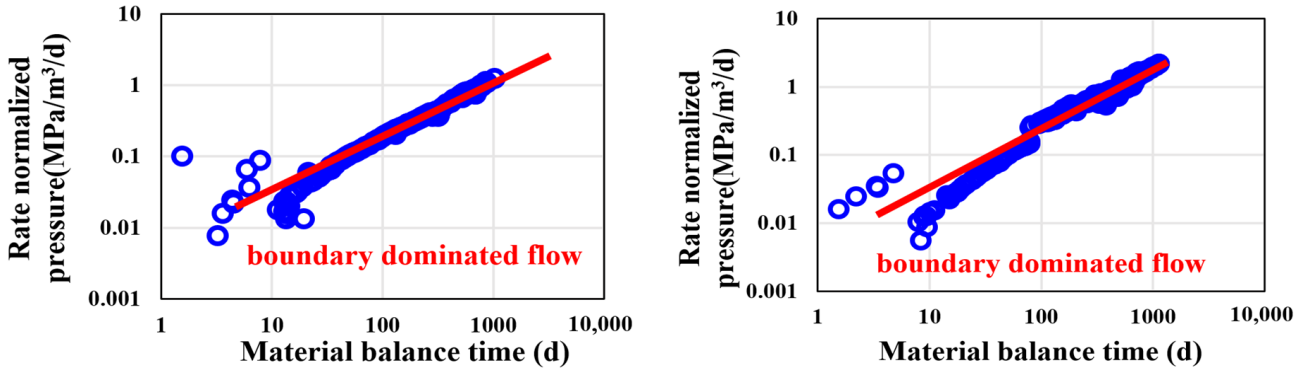


Figure 3. The volume change of the fracture network before and after flowback.

Based on the study of the diagnostic curves of a large number of production wells in typical blocks, it is found that the water phase existing in the finite volume fracture network during the flowback process of shale reservoirs is rapidly discharged under the drive of fracturing elastic energy, and its pressure disturbance can quickly spread to the boundary of the fracture system, and the water phase mostly enters the boundary control flow. The Rate Transient Analysis (RTA) curve of the aqueous phase is shown in Figure 4. In the RTA diagnostic curve, the horizontal axis represents the material balance time, and the vertical axis represents the rate normalized pressure.



(**a**) Water phase diagnosis curve of GY1 well (**b**) Water phase diagnosis curve of GY2 well

Figure 4. Typical well water phase diagnosis curve.

Aiming at the diagnosis and interpretation of water production dynamics in shale reservoirs, a water phase flow model with 'finite conductivity fracture network' as the core can be established. When the flow enters the boundary control flow stage, the corresponding local analytical solution is usually derived based on the material balance principle and the pseudo-steady-state flow assumption, and the local solution of the boundary control flow of the shale reservoir water production dynamic interpretation model is given:

$$\frac{(p_0 - p_w)}{q_w B_w} = \frac{1}{V_f C_{tf}} t \tag{1}$$

where q_w is the water production rate, m^3/d; V_f is the volume of fracture network, m^3; C_{tf} is the comprehensive compression coefficient of fracture, MPa^{-1}; p_0 is pressure at the onset of oil production, MPa; p_w is the flow pressure at the calculation time, MPa; and $B_w = 1$. According to the local solution of the boundary control flow of the shale reservoir water production dynamic interpretation model, the input parameters and output parameters of the productivity evaluation model are derived. The water-phase energy production formula is based on the assumption of boundary-controlled flow.

$$q_w = \frac{(p_0 - p_w) V_f C_{tf}}{t} \tag{2}$$

Based on the dynamic interpretation model of water production in shale reservoirs, the prediction of water production in the boundary control flow stage is mainly based on four types of input parameters: fracture network volume (V_f, obtained by well test data inversion); coefficient of compressibility (C_{tf}, often taken by the empirical value 0.02 MPa^{-1}); production pressure differential (Δp); and production time (t). Both are determined by the actual working system. Using these parameters, the model can calculate and output the key dynamic index-water production rate (q_w), so as to realize the quantitative prediction and dynamic evaluation of water production capacity in this stage.

3.2. Construction of Semi-Empirical Productivity Evaluation Model for Oil Phase

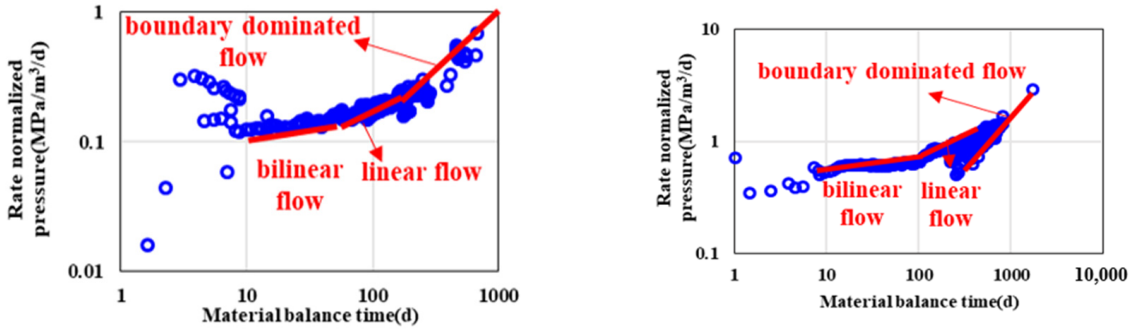
The fracture classification of shale reservoirs is extremely complex [29]. Based on the analysis of the flow mechanism of the complex fracture network system after fracturing in the GuLong shale reservoir, the spatially interwoven horizontal and vertical fracture networks can be equivalent to the basic flow unit composed of the 'fracture segment' and 'fracture-controlled matrix'. The 'fracture section' is the main channel of high conductivity, and the 'fracture-controlled matrix' supplies the flow to the high-conductivity fracture. The two together form a series system in which the matrix supplies liquid to the fracture and the fracture dominates the flow.

The horizontal and vertical complex fracture network of the GuLong shale reservoir is equivalent to the flow unit of fracture section + fracture control matrix. A single fracture unit can be expressed as a series system of matrix + fracture, and a simplified flow physical model is established. The physical model is shown in Figure 5.



Figure 5. Physical model of the oil phase flow.

The dynamic analysis of production wells in the block shows that there are three typical stages of oil phase flow. The slope of the early derivative curve is 1/4, showing the characteristics of 'bilinear flow', which is characterized by the coupled linear flow of the fracture and matrix to the fracture network. The slope of the mid-term derivative curve turns to 1/2, showing the characteristics of 'linear flow', which is mainly the coupling flow along the main fracture boundary and the matrix to the fracture network. In the later stage, the slope of the derivative curve rises to 1, the pressure disturbance affects the entire effective transformation volume boundary, and the flow enters the pseudo-steady-state stage. The RTA curve of the oil phase is shown in Figure 6.



(**a**) Oil phase diagnosis curve of GY1 well (**b**) Oil phase diagnosis curve of GY2 well

Figure 6. Typical well oil phase diagnosis curve.

The early bilinear flow (m = 1/4) has a short duration and mainly reflects the local flow inside the fracture, which has a limited contribution to long-term productivity. The linear flow (m = 1/2) reflects the stable liquid supply process from the fracture-controlled matrix to the fracture system. The boundary control flow stage (m = 1) represents the final state of the overall utilization of the reservoir. These two stages have long durations and stable dynamic characteristics, which characterize the whole process from 'matrix liquid supply' to 'system failure', and are more suitable for productivity formula derivation,

dynamic reserve prediction, and development strategy optimization. This paper mainly derives the production capacity based on the linear flow and boundary control flow stages. Combined with the classical single-phase linear flow basic solution, this solution is applied to the 'fracture–matrix' system of shale reservoirs, and the oil phase productivity evaluation formula considering the fracturing fracture–matrix flow space is constructed. The formula is improved by considering the influence of the gas phase and water phase. Finally, the flow resistance is introduced to simplify the formula.

Dimensionless fundamental solution in the single-phase linear flow stage:

$$\frac{1}{q_D} = \sqrt{\pi t_D} + \frac{\pi}{3C_{FD}} \tag{3}$$

where q_D is dimensionless yield; t_D is dimensionless time; C_{FD} is dimensionless conductivity.

The equation is dimensionalized:

$$\frac{(p_i - p_w)}{q_o B_o} = \frac{\sqrt{\pi} \times 1.842 \times \sqrt{0.0864}\mu_o}{h} \left(\frac{1}{\phi_m \mu_o c_{tm}}\right)^{1/2} \frac{1}{\sqrt{k_m} x_F} t^{1/2} + \frac{\pi x_F \mu_o}{3 \times 1.842 \times (k_F w_F) h} \tag{4}$$

Considering the influence of gas and water on the oil phase, the following is obtained:

$$\frac{(p_i - p_w)}{q_o B_o} = \frac{\sqrt{\pi} \times 1.842 \times \sqrt{0.0864}\mu_o}{h} \left(\frac{1}{\phi_{mo} \mu_o c_{tm}}\right)^{1/2} \frac{1}{\sqrt{k_m k_{mro}(s_g)} n_S x_F} t^{1/2} + \frac{\pi x_F \mu_o}{3 \times 1.842 \times n_S \times (k_F w_F) \times k_{Fro}(s_w) h} \tag{5}$$

The linear production equation of the oil phase under the influence of gas and water is obtained:

$$q_o = \frac{(p_i - p_w)}{\left(\frac{\sqrt{\pi} \times 1.842 \times \sqrt{0.0864}\mu_o}{h} \frac{1}{\sqrt{k_m \phi_m \mu_o c_{tm}} n_S x_F}\right) \times \frac{B_o}{\sqrt{k_{mro}(s_g)}} t^{1/2} + \left(\frac{\pi x_F \mu_o}{3 \times 1.842 \times n_S \times (k_F w_F) h}\right) \times \frac{B_o}{k_{Fro}(s_w)}} \tag{6}$$

where q_o is the oil production rate, m^3/d; k_m is matrix permeability, $\times 10^{-3}$ μm^2; k_F is fracture permeability, $\times 10^{-3}$ μm^2; ϕ_m is the matrix porosity,%; μ_o is the viscosity of the oil phase, mPa·s; C_{tm} is the matrix comprehensive compression coefficient, MPa^{-1}; n_s is the number of fracturing clusters; x_F is half the length of the main fracture, m; w_F is the main fracture width, m; h is the reservoir thickness, m; B_o is the volume coefficient of the oil phase, m^3/m^3; p_i is the initial reservoir pressure, MPa; p_w is the calculation time flow pressure, MPa.

The dynamic flow resistance in the flow of the oil phase linear flow is divided into matrix resistance and fracture resistance. As shown in Figure 7 of the linear flow graph.

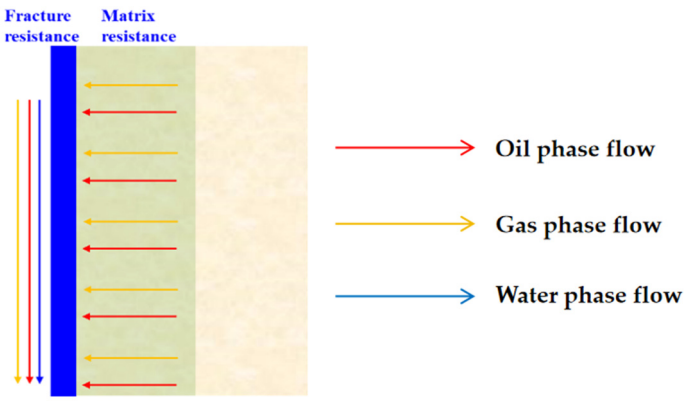


Figure 7. Linear flow method.

Reservoir dynamic flow resistance:

$$R_{mo} = \left(\frac{\sqrt{\pi} \times 1.842 \times \sqrt{0.0864}\mu_o}{h} \frac{1}{\sqrt{k_m \phi_m \mu_o c_{tm}} n_S x_F} \right) \times \frac{B_o}{\sqrt{k_{mro}(s_g)}} t^{1/2} \quad (7)$$

The dynamic flow resistance of pressure fracture:

$$R_{Fo} = \left(\frac{\pi x_F \mu_o}{3 \times 1.842 \times n_S \times (k_F w_F) h} \right) \times \frac{B_o}{k_{Fro}(s_w)} \quad (8)$$

The flow capacity parameters are as follows: $\sqrt{k_\mathrm{m}} A_\mathrm{F} = \sqrt{k_\mathrm{m}} \times 2 n_\mathrm{S} x_\mathrm{F} h$; the fracturing fracture resistance coefficient is as follows: $R_F = \frac{x_F \mu_o}{0.569 \times n_S \times (k_F w_F) h}$.

Therefore, in the linear flow mode, the production capacity formula for the oil phase is as follows:

$$q_o = \frac{(p_i - p_w)}{1.919 \left(\frac{\mu_o}{\phi_m c_{tm}} \right)^{1/2} \frac{1}{\sqrt{k_m} A_F} \frac{B_o}{\sqrt{k_{mro}(s_g)}} t^{1/2} + \frac{R_F B_o}{k_{Fro}(s_w)}} \quad (9)$$

Based on the basic solution of single-phase boundary control flow, the oil phase productivity evaluation formula considering fracturing the fracture–matrix flow space is constructed and simplified.

The fundamental solution of single-phase boundary control flow is as follows:

$$\frac{1}{q_D} = \frac{\pi}{2} t_D \left(\frac{x_f}{y_e} \right) + \frac{\pi}{6} y_{eD} + \frac{\pi}{3 C_{FD}} \quad (10)$$

The equation has the following dimensions:

$$\frac{(p_i - p_w)}{q_o B_o} = \frac{1}{(SRV s_{oi} \phi_m) c_{tm}} t + \frac{\pi}{6} \frac{1.842 \mu_o y_e}{k_{mo} n_S x_F h} + \frac{\pi x_F \mu_o}{3 \times 1.842 \times n_S (k_F w_F) h} \quad (11)$$

The local solution of the dimensional boundary control flow considering the influence of gas and water is as follows:

$$\frac{(p_i - p_w)}{q_o B_o} = \frac{1}{(SRV s_{oi} \phi_m) c_{tm}} t + \frac{\pi}{6} \frac{1.842 \mu_o y_e}{k_m k_{mro}(s_g) n_S x_F h} + \frac{\pi x_F \mu_o}{3 \times 1.842 \times n_S \times (k_F w_F) \times k_{Fro}(s_w) h} \quad (12)$$

The oil phase productivity formula of boundary control flow under the influence of the gas–water two-phase flow is derived:

$$q_o = \frac{(p_i - p_w)}{\frac{B_o}{(SRV s_{oi} \phi_m) c_{tm}} t + \frac{\pi}{6} \frac{1.842 y_e B_o \mu_o}{k_m k_{mro}(s_g) n_S x_F h} + \left(\frac{\pi x_F \mu_o}{3 \times 1.842 \times n_S \times (k_F w_F) h} \right) \times \frac{B_o}{k_{Fro}(s_w)}} \quad (13)$$

where q_o is the oil production rate, m^3/d; k_m is matrix permeability, $\times 10^{-3}$ $\mu\mathrm{m}^2$; k_F is fracture permeability, $\times 10^{-3}$ $\mu\mathrm{m}^2$; ϕ_m is the matrix porosity, %; μ_o is the viscosity of the oil phase, mPa·s; C_tm is the matrix comprehensive compression coefficient, MPa^{-1}; n_s is the number of fracturing clusters; x_F is half the length of the main fracture, m; w_F is the main fracture width, m; h is the reservoir thickness, m; B_o is the volume coefficient of oil phase, $\mathrm{m}^3/\mathrm{m}^3$; p_i is the initial reservoir pressure, MPa; p_w is the calculation time flow pressure, MPa. SRV is the control volume of the fracture, m^3; y_e is the half width of the unit transformation area, m.

During the flow process controlled by the oil phase boundary, the dynamic permeability resistance can be divided into matrix resistance and fracture resistance. The boundary control flow is shown in Figure 8.

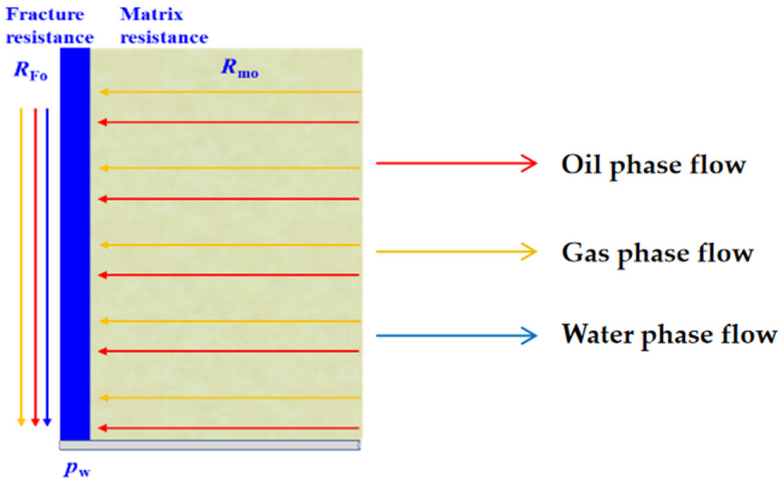


Figure 8. Boundary control flow mode.

Reservoir dynamic flow resistance is as follows:

$$R_{mo} = \left[\frac{1}{(SRVs_{oi}\phi_m)c_{tm}} t + \frac{\pi}{6} \frac{1.842\mu_o y_e}{k_m k_{mro}(s_g) n_S x_F h} \right] B_o \tag{14}$$

The dynamic flow resistance of pressure fracture is as follows:

$$R_{Fo} = \left(\frac{\pi x_F \mu_o}{3 \times 1.842 \times n_S \times (k_F w_F) h} \right) \times \frac{B_o}{k_{Fro}(s_w)} \tag{15}$$

The flow capacity parameters are as follows: $\sqrt{k_\mathrm{m}} A_\mathrm{F} = \sqrt{k_\mathrm{m}} \times 2 n_\mathrm{S} x_\mathrm{F} h$; the fracture resistance coefficient is as follows: $R_F = \frac{x_F \mu_o}{0.569 \times n_S \times (k_F w_F) h}$.

Under the boundary control flow mode, the oil phase productivity formula is as follows:

$$q_o = \frac{(p_i - p_w)}{\frac{B_o}{(SRVs_{oi}\phi_m)c_{tm}} t + \frac{0.964\mu_o B_o}{k_{mro}(s_g)} \left(\frac{1}{\sqrt{k_m} A_F} \right)^2 + \frac{R_F B_o}{k_{Fro}(s_w)}} \tag{16}$$

The key parameter system of shale reservoir productivity prediction and evaluation model is as follows. The input parameters mainly include two categories: one is the material basis parameters (such as horizontal section length, porosity, oil saturation, reservoir thickness, fracture control volume, etc., from geological, fracturing, and well test data); the second is the flow parameters (such as the inverted fracture–matrix composite parameters, fluid properties, and production pressure difference, etc.), which are used to characterize the flow conditions and flow driving forces of the fluid. The output parameter is the production dynamic index of the oil production rate. In addition, the model also introduces three nonlinear matching coefficients of starting pressure gradient, reservoir degassing, and fracture stress sensitivity, which are used to correct the complex nonlinear flow effect in shale reservoirs, so as to improve the accuracy of productivity prediction.

3.3. Construction of Gas Phase Semi-Empirical Productivity Evaluation Model

When the average formation pressure is higher than the saturation pressure of crude oil, the formation crude oil is not degassed, and the production gas–oil ratio (GOR) remains the original dissolved gas–oil ratio (R_{si}). When the average pressure of the formation is lower than the saturation pressure, the dissolved gas in the crude oil begins to eject and

forms a free gas phase. At this time, the gas production consists of two parts: one is the gas still dissolved in the oil, and the other is the free gas ejected.

$$GOR = \frac{q_g / B_g + q_o R_s / B_o}{q_o / B_o} \tag{17}$$

where the following applies:

$$\frac{q_g / B_g + q_o R_s / B_o}{q_o / B_o} = \begin{cases} \frac{\mu_o B_o, k_{rg} + R_s \mu_g B_g k_{ro}}{\mu_g B_g k_{ro}} & p_w \le p \le p_b \\ R_s & p_b \le p \le p_i \end{cases} \tag{18}$$

The relative permeability of oil and gas is related to the average gas saturation. The viscosity and volume coefficients of oil and gas, R_s, are related to the average pressure. GOR is the function of average pressure $\overline{p}$ and average gas saturation $\overline{S}_g$:

$$GOR(\overline{S}_g, \overline{p}) = \frac{q_{gsc}}{q_{osc}} = R_s(\overline{p}) + \frac{k_{mrg}}{k_{mro}}(\overline{S}_g)\frac{\mu_o B_o}{\mu_g B_g}(\overline{p}) \tag{19}$$

Under the condition of degassing after contacting with oil, the gas phase production capacity formula must be based on the accurate prediction of the oil phase production capacity and the GOR. The gas production rate was calculated by GOR and q_o using oil production:

$$q_g = GOR \times q_o \tag{20}$$

Key parameters related to gas production prediction of shale gas reservoirs are as follows. The input parameters mainly include the following: the dissolved gas–oil ratio (R_s) and oil production rate (q_0) in production dynamics; the oil phase and gas phase viscosity (μ_0, μ_g) and volume coefficients (B_0, B_g) from the fluid parameters; and the relative permeability of the oil phase and gas phase from the relative permeability curve (k_{mro}, k_{mrg}). Based on these inputs, the core output parameter of the model is the predicted value of the gas production rate (q_g).

4. Semi-Empirical Productivity Evaluation Model

The unknown parameters in the multiphase semi-empirical productivity evaluation model need to be determined according to other oilfield data. The key input parameters of the semi-empirical formula for oil phase productivity evaluation are as follows: material basis parameters, flowability parameters, modification parameters, and working regime parameters. In addition to matching coefficients, secondary calculation parameters are as follows: oil saturation (S_o), water cut (f_w), Stimulated Reservoir Volume (SRV and $k_m{}^{0.5}A_F$), and nonlinear parameters (n, a, and γ).

4.1. Determination of Oil Saturation

The relationship between oil saturation and production pressure difference is obtained through the P–S relationship curve, and then the oil saturation under each pressure difference can be predicted. This paper is aimed at volatile shale oil reservoirs. During the process of crude oil production, as the pressure decreases, gases will be separated out. The two-phase saturation of oil and gas within the matrix under different pressures can be inverted from the production gas–oil ratio, thereby correcting the multiphase problem of the semi-empirical model.

The shale matrix is extremely tight, and the compressibility relative to oil and gas is negligible. Through the accumulation term, the characterization equation of oil and gas

two-phase production is constructed, and the cumulative underground gas production is as follows:

$$V_g = \frac{S_g V_p}{B_g} + \frac{R_s V_p (1 - S_g)}{B_o} \tag{21}$$

The cumulative oil production underground is as follows:

$$V_o = \frac{V_p (1 - S_g)}{B_o} \tag{22}$$

Under a given pressure, the ratio of gas to oil production can be expressed in the following two forms:

First, based on the material balance equation, the gas–oil ratio is expressed as follows:

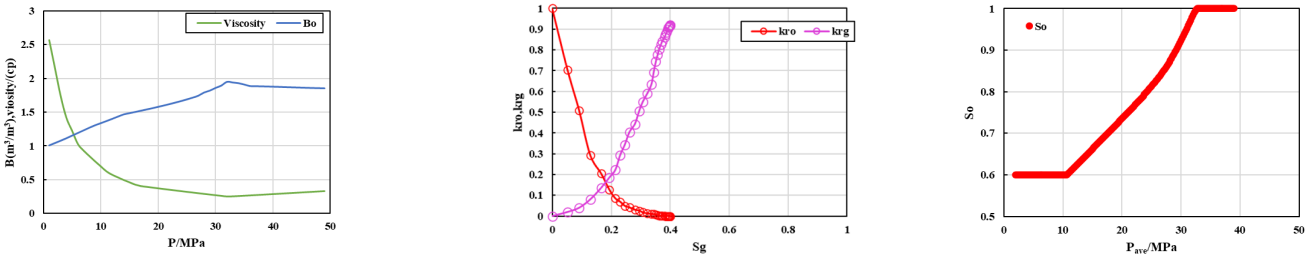
$$R_p = \frac{\mathrm{d}V_g/dp}{\mathrm{d}V_o/dp} = -\frac{\frac{1}{B_g}\frac{dS_g}{dp} - \frac{S_g}{B_g^2}\frac{dB_g}{dp} - \frac{R_s}{B_o}\frac{dS_g}{dp} + \frac{(1-S_g)}{B_o}\frac{dR_s}{dp} - \frac{R_s(1-S_g)}{B_o^2}\frac{dB_o}{dp}}{\frac{(1-S_g)}{B_o^2}\frac{\mathrm{d}B_o}{\mathrm{d}p} + \frac{1}{B_o}\frac{\mathrm{d}S_g}{\mathrm{d}p}} \tag{23}$$

Second, the gas–oil ratio derived from the formula of the two-phase motion equation of oil and gas is as follows:

$$R_p = \frac{Q_g/B_g + Q_o R_s/B_o}{Q_o/B_o} = \begin{cases} \frac{\mu_o B_o k_{rg} + R_s \mu_g B_g k_{ro}}{\mu_g B_g k_{ro}} & p_w \le p \le p_b \\ R_s & p_b \le p \le p_i \end{cases} \tag{24}$$

The parameters in the formula are classified as follows: the PVT parameters of the oil–gas two-phase nano-space and the nano-space oil–gas phase permeability parameters. Both of these two types of parameters are measurable in the laboratory and have high certainty. Different pressure and gas saturation data are substituted into the formula for calculation, and the relationship between pressure and saturation in the nano-matrix can be obtained, as shown in Figure 9.

$$\frac{dS_g}{dp} = \frac{\frac{S_g}{B_g}\frac{dB_g}{dp} - \frac{\mu_o k_{rg}}{\mu_g k_{ro}}\frac{(1-S_g)}{B_o}\frac{\mathrm{d}B_o}{\mathrm{d}p} - \frac{(1-S_g)B_g}{B_o}\frac{dR_s}{dp}}{1 + \frac{\mu_o k_{rg}}{\mu_g k_{ro}}} \tag{25}$$



(**a**) PVT parameters in the nanoscale

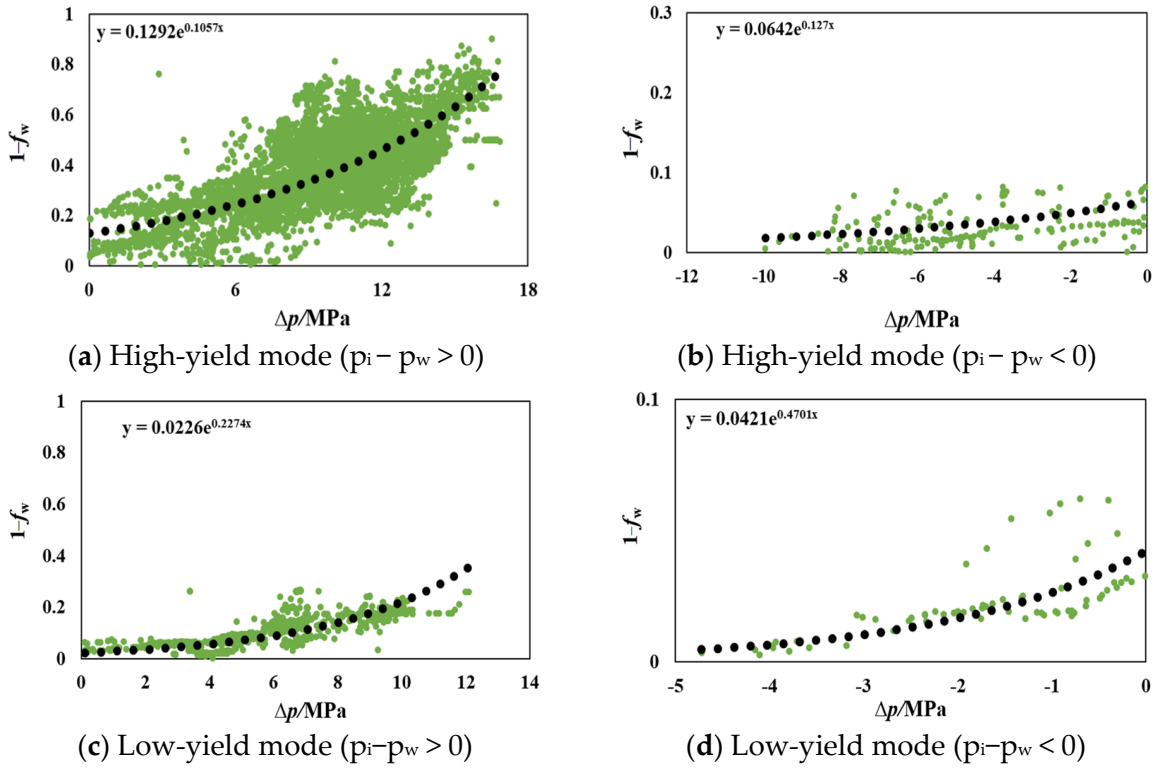
(**b**) Oil–gas phase permeability in the nanoscale

(**c**) P-S relationship in the nanoscale

Figure 9. P-S Relationship Curve.

4.2. Determination of Water Cut fw

The relationship between the water cut f_w and production pressure difference Δp was obtained through statistical methods, and the water cut under each pressure difference was predicted, as shown in Figure 10.



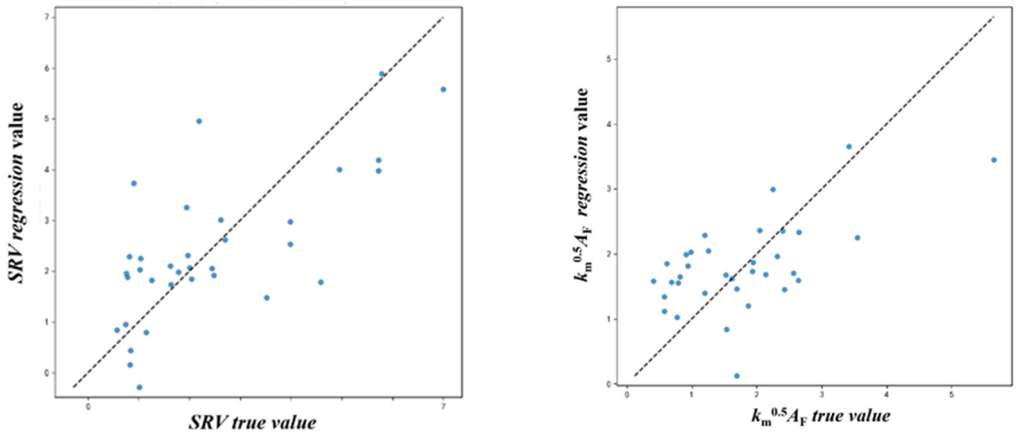
(**a**) High-yield mode ($p_i - p_w > 0$) (**b**) High-yield mode ($p_i - p_w < 0$)

(**c**) Low-yield mode ($p_i - p_w > 0$) (**d**) Low-yield mode ($p_i - p_w < 0$)

Figure 10. Relationship between water content f_w and Δp.

4.3. Determination of the Stimulated Reservoir Volume SRV and $k_m^{0.5}A_F$

The RTA method was used to conduct parameter inversion for 51 production wells, and the SRV and $k_m^{0.5}A_F$ were obtained. Based on the parameters of these 51 production wells, an empirical regression was carried out, and the empirical formulas for SRV and $k_m^{0.5}A_F$ were respectively obtained, as shown in Figure 11.



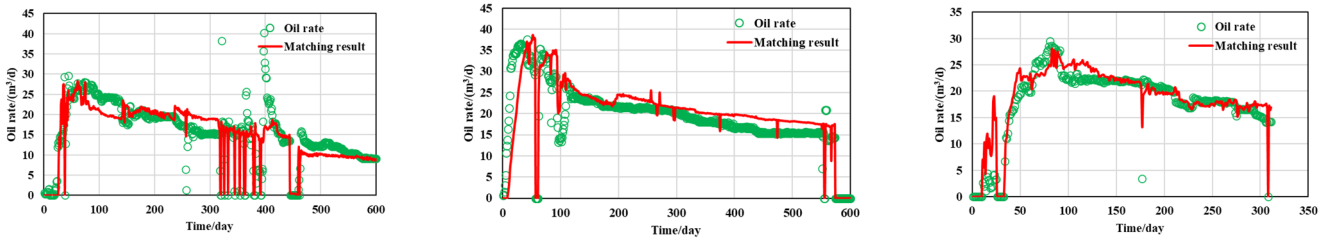
(**a**) SRV regression results (**b**) $k_m^{0.5}A_F$ regression results

Figure 11. Regression results of stitched volume SRV and $k_m^{0.5}A_F$.

4.4. Determination of Nonlinear Parameters

The nonlinear parameters include the following: n, the nonlinear flow index, where $n \in (0.5–1)$; a, the nonlinear parameter caused by reservoir degassing, where $a \in (0–0.5)$; γ, the stress-sensitive parameter of fracture conductivity, where $\gamma \in (0–0.5)$. Based on the petroleum production data of 51 production wells from the same oil layer in the same oil field, the matching parameters were obtained, as shown in Figure 12: $n = 0.95$, $a = 0.032$,

$\gamma = e^{-0.3}$. The initial oil saturation of the matrix is relatively high, at 0.7. The initial water saturation of the crack was relatively high, at 0.8.



(**a**) W1 well matching (**b**) W2 well matching (**c**) W3 well matching

Figure 12. Parameters of nonlinear fitting for some wells.

While numerical approaches such as Discrete Fracture Models (DFM) or Embedded Discrete Fracture Models (EDFM) offer high precision, their computational cost grows exponentially as the number of grid cells increases, and the simulation performance is often sensitive to grid quality. In contrast, the semi-empirical model proposed in this study functions essentially as a two-grid system that requires no iterative calculations. This leads to a qualitative leap in computational efficiency compared to traditional numerical simulations, making it particularly suitable for rapid field-scale evaluations.

4.5. Production Calculation Method

Based on the above matching results, the three-phase production capacity can be calculated separately. The calculation formulas are as follows:

The formula for calculating the water rate is as follows:

$$q_w = \frac{V_f C_{tf}}{B_w t}(p_0 - p_w) \tag{26}$$

The formula for calculating the oil phase is as follows. When $p_{wf} < p_i$, the oil phase mainly emerges through the pressure fractures and is calculated using an empirical formula:

$$q_o = q_w \frac{1 - f_w(p_i - p_w)}{f_w(p_i - p_w)},\ p_i \le p_w \tag{27}$$

When $p_{wf} > p_i$, the oil phase mainly emerges from the reservoir. The calculation is done using the matching formula:

$$q_o = \begin{cases} \dfrac{(p_i - p_w)^n}{1.919\left(\frac{\mu_o}{\phi_m c_{tm}}\right)^{1/2} \frac{1}{\sqrt{k_m} A_F} \frac{B_o}{(s_o)^a} t^{1/2} + \frac{R_F^\gamma B_L}{f_w}} & ,t \le 0.482\phi_m \mu_o c_{tm}\left(\frac{SRV}{\sqrt{k_m} A_F}\right)^2 \\ \dfrac{(p_i - p_w)^n}{\frac{B_o}{(SRVs_{oi}\phi_m)c_{tm}} t + \frac{0.964\mu_o B_o}{k_{mro}(s_o)^a}\left(\frac{1}{\sqrt{k_m} A_F}\right)^2 + \frac{R_F^\gamma B_L}{f_w}} & ,t > 0.482\phi_m \mu_o c_{tm}\left(\frac{SRV}{\sqrt{k_m} A_F}\right)^2 \end{cases} \tag{28}$$

The gas phase production calculation formula is as follows. First, the gas–oil ratio needs to be calculated:

$$GOR = \begin{cases} \dfrac{\mu_o B_o k_{rg} + R_s \mu_g B_g k_{ro}}{\mu_g B_g k_{ro}} & \overline{p} < p_b \\ R_s & \overline{p} \ge p_b \end{cases} \tag{29}$$

Then, the actual gas yield can be calculated based on the oil yield. The specific formula is shown in Equation (20).

4.6. Numerical Simulation Verification

This section mainly uses the tNavigator model to verify the accuracy of the production capacity calculation of the semi-empirical model presented in this paper. The model is for a fractured horizontal well in a shale oil reservoir. The basic model is shown in Figure 13, which is a schematic diagram of the numerical model. The tNavigator model uses a total of 35,600 grids. Establishment of the numerical model is as follows:

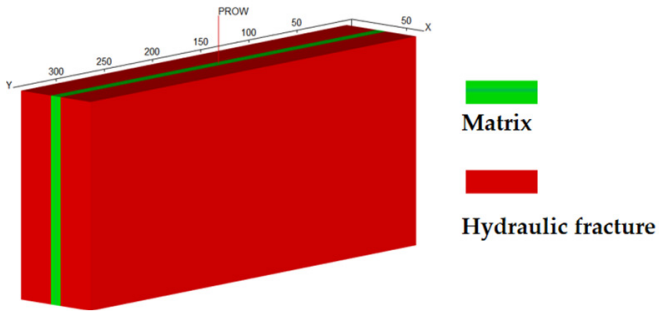
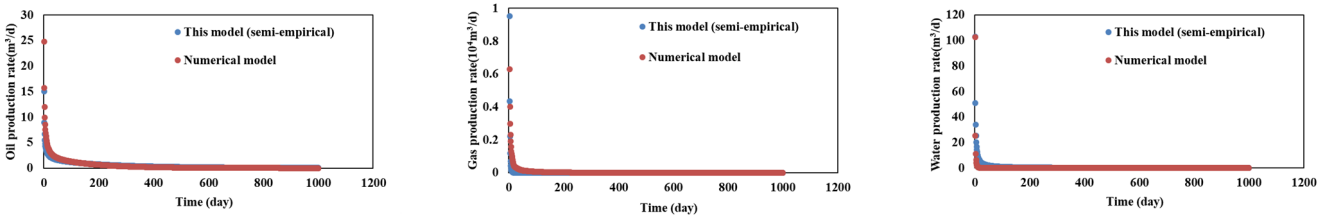


Figure 13. Three-dimensional numerical simulation graph.

First, the tNavigator model was used to calculate the daily oil production, daily gas production, and daily water production of this fractured horizontal well within 1000 days. Some data points were taken during these 1000 days, and the bottom-hole flow pressure calculated by the tNavigator model was input into the model in this paper to calculate the daily oil production, daily gas production, and daily water production. Figure 14a shows the comparison curve of daily oil production between the model in this paper and the tNavigator model. Figure 14b shows the comparison curve of daily gas production between the model in this paper and the tNavigator model. Figure 14c shows the comparison curve of daily water production between the model in this paper and the tNavigator model. It can be seen that the curves of daily oil production, daily gas production, and daily water production are highly consistent throughout the process. However, numerical simulation cannot consider the influence of engineering parameters and the calculation speed is relatively slow, while the semi-empirical model in this paper can consider shale oil reservoirs under the influence of engineering parameters and improve the calculation efficiency.



(**a**) Oil production rate (**b**) Gas production rate (**c**) Water production rate

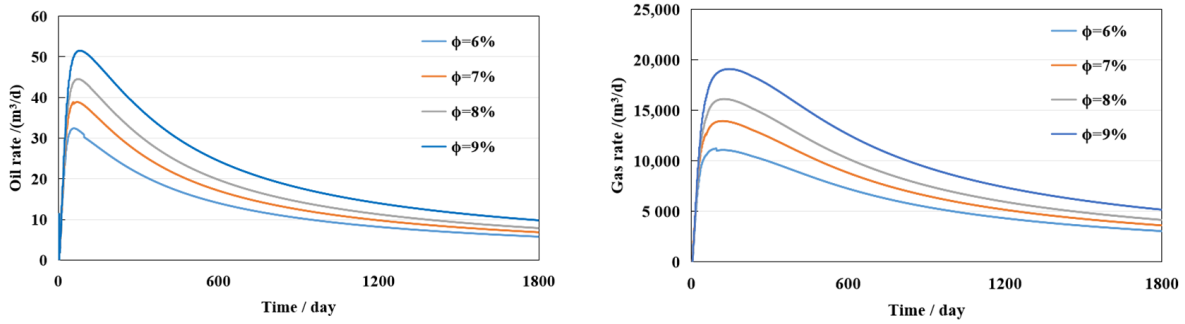
Figure 14. Comparison of the numerical model and the model in this article.

5. Research on Productivity Laws Under Different Factors

The productivity of shale oil is affected by factors such as the reservoir, construction, and production system. To further clarify the main controlling factors of shale oil productivity, based on the established multiphase semi-empirical productivity evaluation model for shale oil reservoirs, the influence of geological reservoir parameters, fracturing parameters, working system parameters, and nonlinear parameters on the oil and gas rate is studied. The variation patterns and characteristics of productivity under the influence of a single factor are analyzed.

5.1. Geologic Parameter Analysis

As shown in Figure 15, matrix porosity is a key physical parameter characterizing the reservoir's storage capacity. Its magnitude directly affects the effective permeability and fracture-controlled reserves of the reservoir, and its impact on production is continuous throughout the entire cycle. With the increase in matrix porosity, the pore space for fluid storage and flow in the reservoir increases, the absolute permeability of the reservoir increases, the flow efficiency of fluid in the matrix is significantly improved, and the total oil and gas reserves that can be stored in the fracture control volume also increase accordingly, which makes the peak oil production rise steadily with the increase in matrix porosity. Matrix porosity significantly influences the whole production cycle, the core reason being that the absolute permeability is the key throughout the whole development phase percolation index, whether in the early development rapid release of energy, in the middle of the smooth production, or late in the remaining reserves of mining. All rely on the permeability support provided by the matrix porosity. Its influence does not diminish as the development progresses and always acts throughout the entire process of fluid seepage. The gas rate characteristics are similar to those of the oil rate. The greater the porosity, the greater the peak gas production.



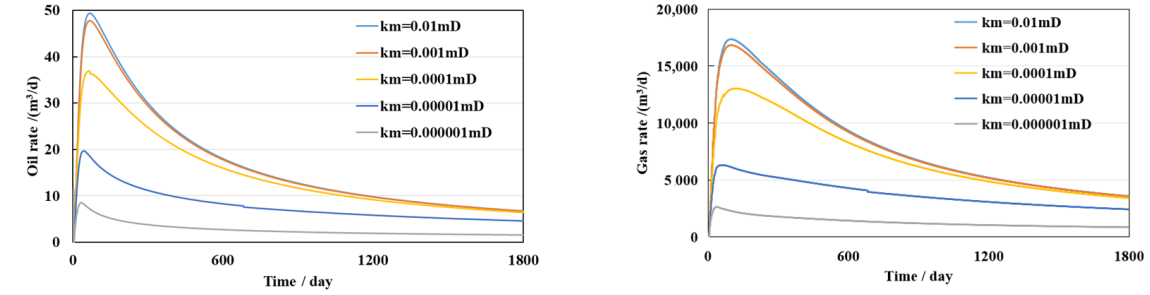
(**a**) Effect of porosity on oil rate (**b**) Effect of porosity on gas rate

Figure 15. Effect of porosity on productivity.

Reservoir permeability affects $k_m^{0.5}A_F$. As shown in Figure 16, the peak oil production increases with the increase in reservoir permeability, and it has an impact on the production throughout the entire period. The higher the reservoir permeability, the smaller the flow resistance of fluids in the reservoir matrix will be, and the higher the migration efficiency of oil and gas from the reservoir matrix to fractures and then to the wellbore. This enhances the effective supply capacity of the matrix to fractures, and the peak oil production will significantly increase with the increase in reservoir permeability. Meanwhile, reservoir permeability has a significant impact on the full-cycle production. Whether it is the peak production capacity in the early stage of development, the control of production decline in the middle stage, or the exploitation of remaining reserves in the later stage, permeability directly determines the fluid migration efficiency. The gas rate characteristics are similar to those of the oil rate. The greater the permeability, the greater the peak gas rate.

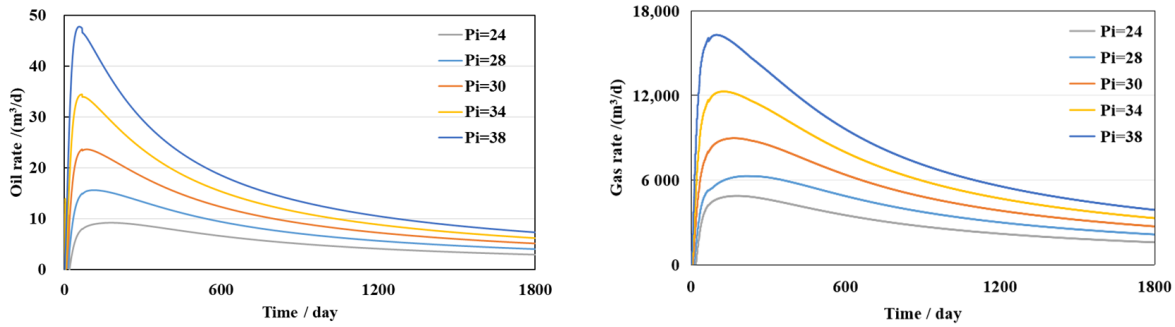
The initial formation pressure affects the production pressure difference. As shown in Figure 17, the peak oil production increases with the increase in the initial formation pressure, and it has an impact on the total production throughout the cycle. The greater the initial formation pressure, under the same production conditions (such as bottom-hole flowing pressure, production string parameters, etc.), the greater the production pressure difference (the difference between the initial formation pressure and the bottom-hole flowing pressure) will be, and the production pressure difference is the core driving force for the flow of fluids from the reservoir to the wellbore. The greater the pressure difference,

the faster the fluid flow rate will be, and the higher the peak production capacity will be. In addition, in the middle and later stages of development, sufficient formation energy can effectively delay the decline in production. The gas rate characteristics are similar to those of the oil rate. The greater the reservoir pressure, the greater the peak gas rate.



(**a**) Effect of matrix permeability on oil rate (**b**) Effect of matrix permeability on gas rate

Figure 16. Effect of reservoir permeability on productivity (k_m is matrix permeability).

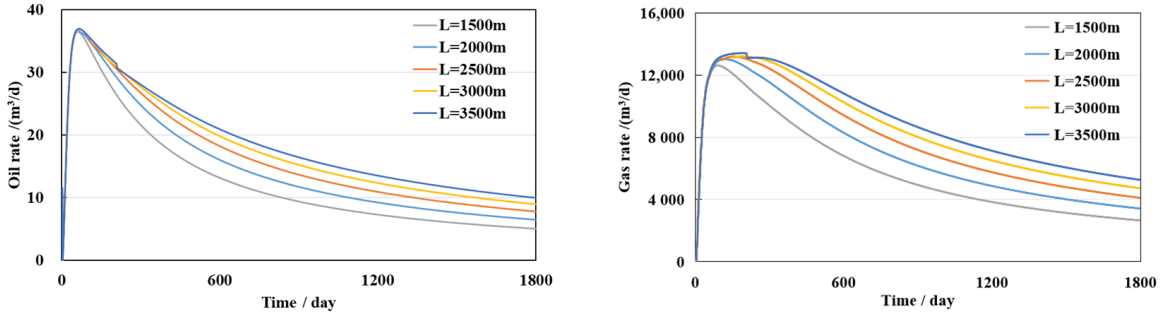


(**a**) Effect of P_i on oil rate (**b**) Effect of P_i on gas rate

Figure 17. Effect of the initial reservoir pressure on productivity.

5.2. Fracturing Parameters Analysis

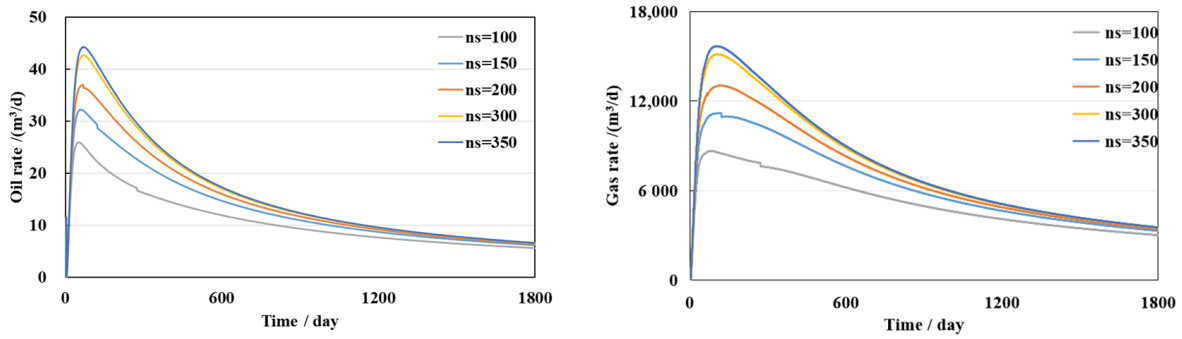
The length of the horizontal section affects the controlled volume of the wellbore. As shown in Figure 18, the length of the horizontal section has a relatively small impact on the peak oil production volume, and has a significant effect on the production in the middle and later stages. A longer horizontal section can continuously provide more sufficient channels for fluid flow in the middle and later stages when the reservoir energy gradually decreases, effectively delaying the decline rate of production and ensuring the stability of production in the middle and later stages. The gas rate characteristics are similar to those of the oil rate; a higher length of the horizontal section correlates with a greater peak gas rate.



(**a**) Effect of L on oil rate (**b**) Effect of L on gas rate

Figure 18. Effect of length of the horizontal section on productivity.

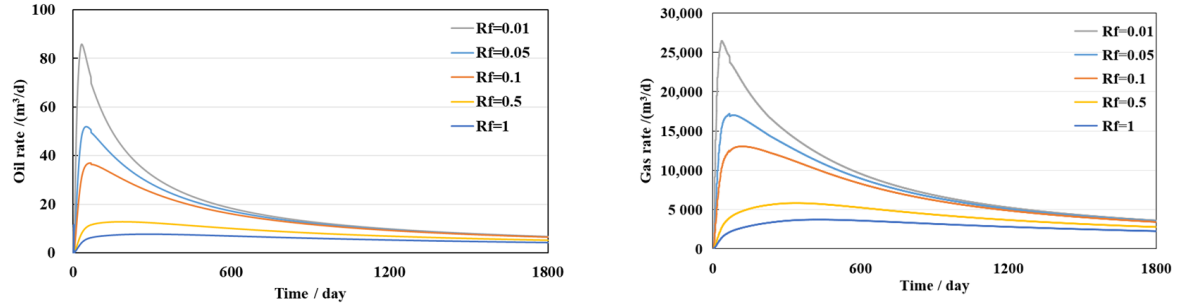
The number of fracture clusters n_s affects $k_m^{0.5}A_F$. As shown in Figure 19, the peak oil production increases with the increase in the number of fracture clusters n_s, which mainly affects the early and middle production. The increase in the number of fracturing clusters means that the distribution density of fractures in the horizontal section is enhanced, and the effective modification range is further expanded, which leads to an improvement in the $k_m^{0.5}A_F$ parameter value. In the early and middle stages of development, the drainage advantage brought by multiple clusters of fractures is most prominent, which can fully utilize the initial production capacity of the reservoir. However, in the later stage, as the fractures gradually close and the reservoir energy decays, the advantage of the number of fracturing clusters will gradually weaken, and the impact on production will also decrease. The gas rate characteristics are similar to those of the oil rate. The larger the number of fracturing clusters, the greater the peak gas production.



(**a**) Effect of n_s on oil rate (**b**) Effect of n_s on gas rate

Figure 19. Effect of the number of fracture clusters n_s on productivity.

The fracture resistance coefficient R_f affects the fracture resistance. As shown in Figure 20, the peak oil production decreases with the increase in the fracture resistance coefficient R_f, which affects the early and middle production. The main reason is that the early and middle production is large, and the fluid flow is mainly concentrated inside the fracture, and the influence of the drag coefficient directly affects the fluid seep from the fracture to the wellbore. However, in the later stage of development, the reservoir energy decreases significantly, and the production is mainly controlled by the remaining reserves and matrix percolation capacity, and the relative influence of fracture resistance coefficient R_f will gradually decrease. The gas rate characteristics are similar to those of the oil rate. The smaller the fracture resistance coefficient R_f is, the greater the peak gas rate will be.

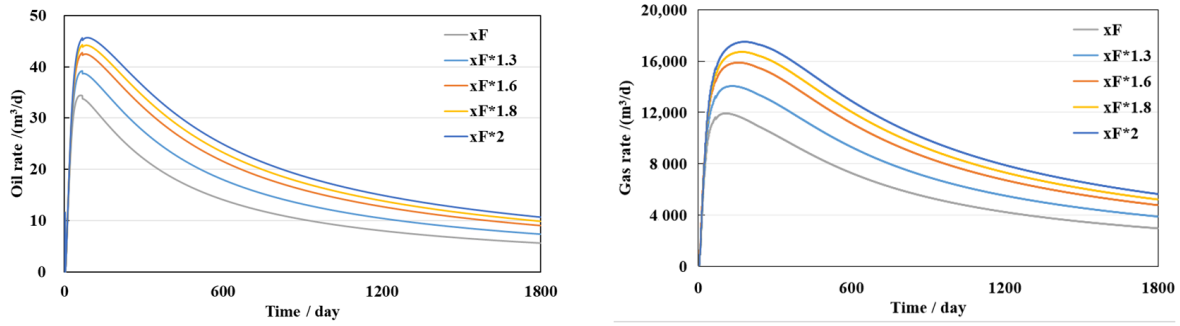


(**a**) Effect of R_f on oil rate (**b**) Effect of R_f on gas rate

Figure 20. Effect of the fracture resistance coefficient R_f on productivity.

The half-length of the fractures, x_F, affects $k_m^{0.5}A_F$ and the controlled volume of the fractures. As shown in Figure 21, the peak oil production increases with the increase in the fracture half-length, and it has an impact on the total production throughout the cycle.

The longer the fracture half-length, the wider the extension range of the fracture into the reservoir. On the other hand, it can also increase the value of the $k_m^{0.5}A_F$ parameter and enhance the effective supply capacity of the fractures. Similar to the horizontal segment length, the fracture half-length has a significant impact on the total production throughout the cycle. In the middle and later stages of development, the expanded controlled volume of the fractures can continuously support production and delay the decline in production. The gas rate characteristics are similar to those of the oil rate. The smaller the fracture resistance coefficient is, the greater the peak gas rate will be.



(**a**) Effect of x_F on oil rate (**b**) Effect of x_F on gas rate

Figure 21. Effect of the half-length of the fractures, x_F, on productivity.

5.3. Work System Parameters Analysis

The work system in shale oil development was summarized, and three patterns of well bottom flow pressure changes were identified: high pressure, medium pressure, and low pressure, as shown in Figure 22. They represent the situations where the formation is non-degassed, slightly degassed, and fully degassed, respectively.

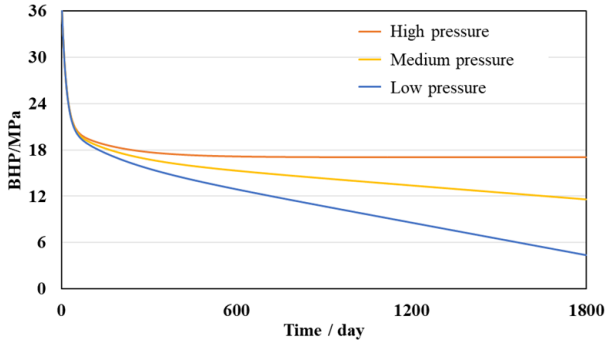
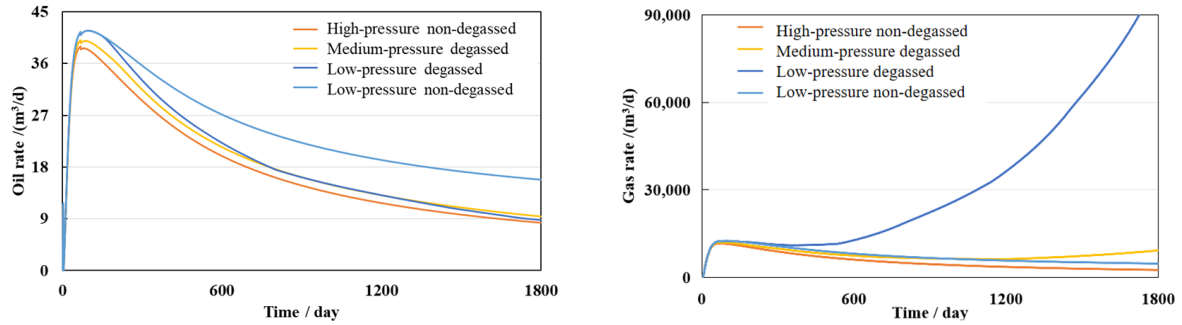


Figure 22. Variation pattern of bottom-hole flow pressure.

The production dynamics under four production regimes—high-pressure non-degassed, medium-pressure degassed, low-pressure degassed, and low-pressure non-degassed—were studied. As shown in Figure 23, the peak production of the oil phase increased as the bottom-hole pressure decreased. At the same time, degassing is also a major factor affecting the oil rate. The peak oil rates in the low-pressure degassed and low-pressure non-degassed systems were equal, but degassing led to a rapid decrease in peak production followed by a significant drop in oil rate. This was because in the degassed state, the formation pressure was significantly lower than the saturation pressure, and a large amount of dissolved gas was released, forming two-phase fluid flow of oil and gas. The presence of the gas phase would significantly increase the fluid flow resistance, and at the same time, the viscosity of the crude oil increased, resulting in a significant decrease in the oil rate, but the gas rate increased significantly.

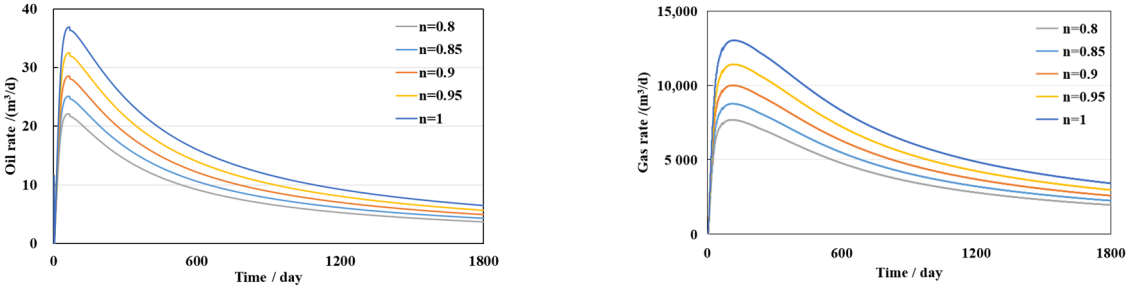


(**a**) The impact of BHP on oil rate (**b**) The impact of BHP on gas rate

Figure 23. Analysis of factors affecting working system parameters.

5.4. Nonlinear Parameters Analysis

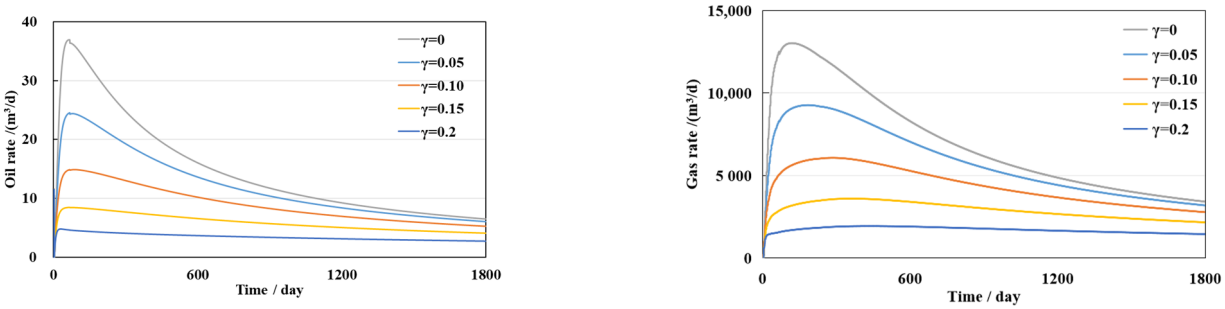
The confined space at the nanoscale exhibits distinct flow characteristics [30], and factor analysis can be conducted by adjusting the nonlinear parameters. The value n represents the influence of reservoir stress sensitivity and the startup pressure gradient on production. As shown in Figure 24, the peak oil rate increases with the increase in the n value, and it has an impact on the total production throughout the cycle. The increase in n value indicates that the stress sensitivity effect of the reservoir is weakened, the starting pressure threshold is reduced, the flow resistance of the fluid in the reservoir matrix is reduced, the migration efficiency of oil and gas from the reservoir to the fracture is significantly improved, and the peak oil rate steadily increases with the increase in the n value. The n value has a significant and continuous impact on the full-cycle production of the oil reservoir. The core reason lies in the fact that the effects of reservoir stress sensitivity and the initiation pressure gradient run through the entire development stage.



(**a**) Effect of reservoir stress sensitivity on oil rate (**b**) Effect of reservoir stress sensitivity on gas rate

Figure 24. Effect of the nonlinear flow index n on productivity.

γ represents the influence of pressure-fracture stress sensitivity on production. As shown in Figure 25, the peak oil production decreases as the γ value increases, and it has an impact on the early and mid-term production. The increase in the γ value indicates that the degree of stress sensitivity affecting the pressure fractures intensifies, and the effective conductivity of the fractures will subsequently decrease. The flow resistance of fluids within the fractures increases, and therefore, the peak oil rate shows a gradually decreasing trend as the γ value increases. This is because in the early and middle stages of development, the reservoir production is greatly influenced by the conductivity of the pressure fractures, and the decline in the conductivity of the fractures will directly and rapidly be reflected in the production; while in the later stage of development, reservoir characteristics become the main controlling factor for production capacity, and the influence of stress sensitivity of the pressure fractures will gradually weaken, and the influence of the γ value on production will also decrease accordingly.

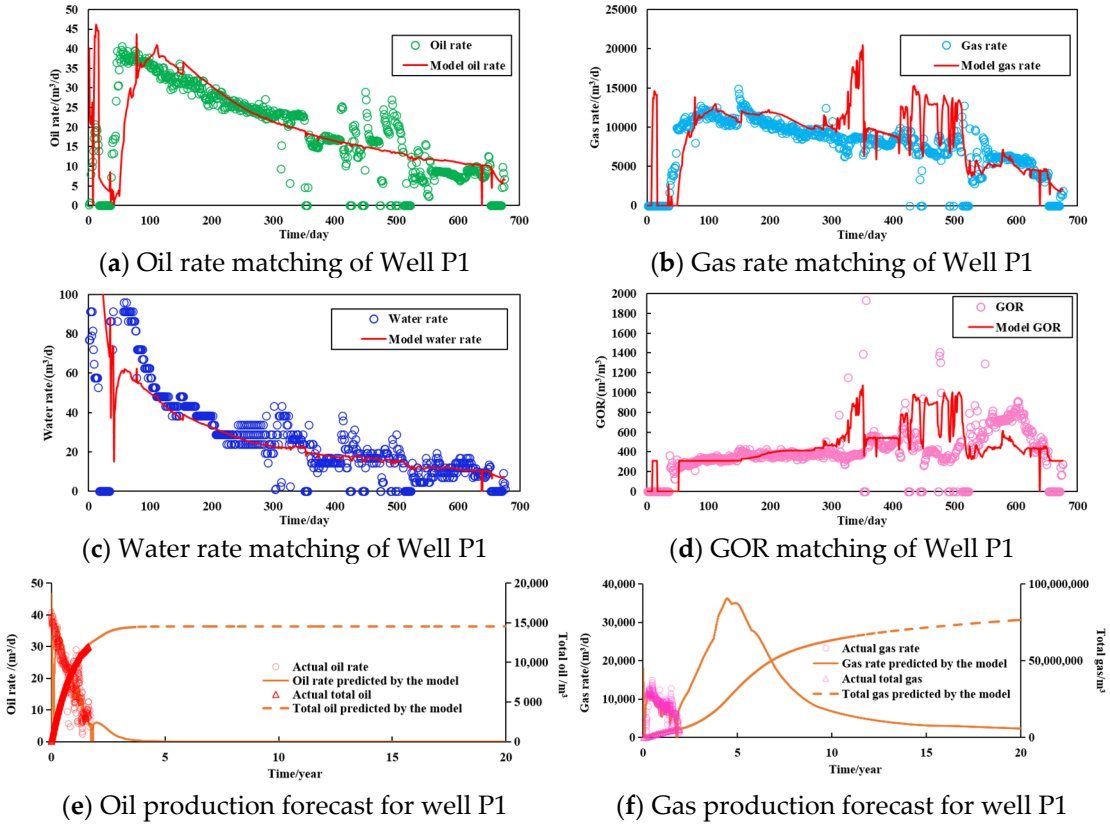


(**a**) Effect of pressure-fracture stress sensitivity on oil rate (**b**) Effect of pressure-fracture stress sensitivity on gas rate

Figure 25. Effect of the pressure-fracture stress sensitivity γ on productivity.

5.5. Historical Matching and Production Dynamics Prediction

Using the constructed semi-empirical production capacity evaluation model in Equations (26)–(30) for oil, gas, and water, the production history of oil, gas, and water, as well as the gas–oil ratio history of wells P1 and P2 were fitted. The matching results are shown in Figures 26a–d and 27a–d. The semi-empirical production capacity evaluation model for oil, gas, and water has a high degree of matching for the three phases of oil, gas, and water, with a compliance rate of over 84% The relative errors for wells P1 and P2 are 15% and 10%, respectively. To a certain extent, this demonstrates the reliability and applicability of the semi-empirical production capacity evaluation model for oil, gas, and water constructed in this paper. In addition to its use on the above typical wells, when this method was applied to other production wells in the same oilfield, the average matching rate was as high as over 81%. The lowest matching rate also reached 80%, which met the engineering requirements. Thus, it can be seen that the model in this paper is applicable to the GuLong oilfield.

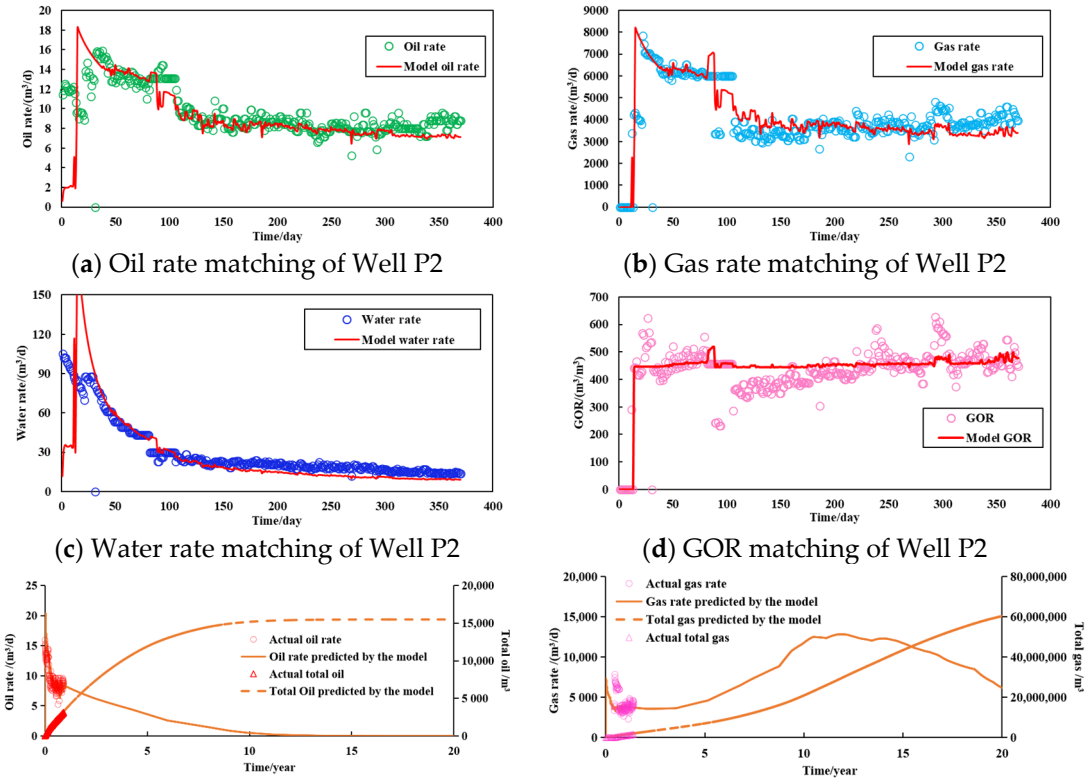


(**a**) Oil rate matching of Well P1 (**b**) Gas rate matching of Well P1

(**c**) Water rate matching of Well P1 (**d**) GOR matching of Well P1

(**e**) Oil production forecast for well P1 (**f**) Gas production forecast for well P1

Figure 26. Historical matching and production prediction of Well P1 using the model.



(**a**) Oil rate matching of Well P2 (**b**) Gas rate matching of Well P2

(**c**) Water rate matching of Well P2 (**d**) GOR matching of Well P2

(**e**) Oil production forecast for well P2 (**f**) Gas production forecast for well P2

Figure 27. Historical matching and production prediction of Well P2 using the model.

In addition, the semi-empirical production capacity evaluation model constructed in this paper can be used to predict the production of oil and gas in the later stage of development. The predicted production of oil and gas for wells P1 and P2 after 20 years of development is provided, as shown in Figure 26e,f and Figure 27e,f.

6. Conclusions

In this paper, the production dynamics of a shale reservoir are combined with the flow mechanism, and the three-phase productivity evaluation formula of oil, gas, and water considering the flow mechanism is constructed. The complex flow mechanism is simplified into different coefficients, and these coefficients are determined using the production dynamics data. A multiphase semi-empirical productivity evaluation method for shale oil reservoirs based on production dynamics and flow mechanism has been developed. An analysis of the factors was conducted, and it was clarified that geological parameters, fracturing parameters, working regime, and nonlinear parameters all have an impact on the productivity of oil and gas mixtures. Porosity, permeability, and initial formation pressure all have an influence on the peak oil rate and the subsequent deceleration rate. The length of the horizontal section affects the later productivity, the number of fracturing clusters and the fracture resistance coefficient affect the peak oil rate, and the length of the pressure-fracturing crack affects the productivity throughout the entire cycle. The production pressure difference has an impact on the peak oil rate and the subsequent deceleration rate, and degassing affects the later oil and gas rate. The nonlinear flow index n has an impact on the total production volume. The stress-sensitive parameter γ of the fracture conductivity capacity has a significant influence on the early and middle stage production. The model shows high accuracy in the history matching of shale oil wells in the field, and can realize the production dynamic prediction of shale oil wells. The

constructed model is of great significance for the rapid evaluation of shale oil production after fracturing.

Author Contributions: Conceptualization, R.W. and H.L.; methodology, R.W.; software, R.W.; validation, R.W. and H.L.; formal analysis, R.W.; investigation, R.W.; resources, R.W.; data curation, R.W.; writing—original draft preparation, R.W.; writing—review and editing, R.W.; visualization, R.W.; supervision, R.W.; project administration, R.W.; funding acquisition, H.L. All authors have read and agreed to the published version of the manuscript.

Funding: This research was funded by the National Science and Technology Major Project Exploration and Development Technology and Integrated Demonstration of Cretaceous Continental Shale Oil in Songliao Basin, grant number 2024ZD1404900.

Data Availability Statement: All data are available within the article.

Conflicts of Interest: Author Rui Wang was employed by the State Key Laboratory of Continental Shale Oil (SKL-CSO) and PetroChina Daqing Oilfield Co., Ltd.; author He Liu was employed by the State Key Laboratory of Continental Shale Oil (SKL-CSO) and PetroChina Research Institute of Petroleum Exploration & Development. The authors declare that the research was conducted in the absence of any commercial or financial relationships that could be construed as a potential conflict of interest.

References

1. Ibrahim, M.; Wattenbarger, R.A. Analysis of Rate Dependence in Transient Linear Flow in Tight Gas Wells. In Proceedings of the Abu Dhabi International Petroleum Exhibition and Conference, Abu Dhabi, United Arab Emirates, 5–8 November 2006. [CrossRef]
2. Ibrahim, M.; Wattenbarger, R.A. Rate Dependence of Transient Linear Flow in Tight Gas Wells. *J. Can. Pet. Technol.* **2006**, *45*, PETSOC-06-10-TN2. [CrossRef]
3. Ilk, D.; Currie, S.M.; Symmons, D.; Rushing, J.A.; Blasingame, T.A. Hybrid Rate-Decline Models for the Analysis of Production Performance in Unconventional Reservoirs. In Proceedings of the SPE Annual Technical Conference and Exhibition, Florence, Italy, 19–22 September 2010. [CrossRef]
4. Valkó, P.P.; Lee, W.J. A Better Way to Forecast Production from Unconventional Gas Wells. In Proceedings of the SPE Annual Technical Conference and Exhibition, Florence, Italy, 19–22 September 2010. [CrossRef]
5. Duong, A.N. An Unconventional Rate Decline Approach for Tight and Fracture-Dominated Gas Wells. In Proceedings of the Canadian Unconventional Resources and International Petroleum Conference, Calgary, AB, Canada, 19–21 October 2010. [CrossRef]
6. Clark, A.J.; Lake, L.W.; Patzek, T.W. Production Forecasting with Logistic Growth Models. In Proceedings of the SPE Annual Technical Conference and Exhibition, Denver, CO, USA, 30 October–2 November 2011. [CrossRef]
7. Currie, S.M.; Ilk, D.; Blasingame, T.A.; Symmons, D. Application of the "Continuous Estimation of Ultimate Recovery" Methodology to Estimate Reserves in Unconventional Reservoirs. In Proceedings of the Canadian Unconventional Resources and International Petroleum Conference, Calgary, AB, Canada, 19–21 October 2010. [CrossRef]
8. Xie, X.; Fairbanks, M.D.; Fox, K.S.; Koinis, R.L. A New Method for Earlier and More Accurate EUR Prediction of Haynesville Shale Gas Wells. In Proceedings of the SPE Annual Technical Conference and Exhibition, San Antonio, TX, USA, 8–10 October 2012. [CrossRef]
9. Al-Ahmadi, H.A.; Almarzooq, A.M.; Wattenbarger, R.A. Application of Linear Flow Analysis to Shale Gas Wells—Field Cases. In Proceedings of the SPE Unconventional Gas Conference, Pittsburgh, PA, USA, 23–25 February 2010. [CrossRef]
10. Brown, M.; Ozkan, E.; Raghavan, R.; Kazemi, H. Practical Solutions for Pressure-Transient Responses of Fractured Horizontal Wells in Unconventional Shale Reservoirs. *SPE Res. Eval. Eng.* **2011**, *14*, 663–676. [CrossRef]
11. Wu, Y.H.; Cheng, L.S.; Huang, S.J.; Xue, Y.C.; Ding, G.Y. A Semi-Analytical Method of Production Prediction for Shale Gas Wells Considering Multi-Nonlinearity of Flow Mechanisms. *Sci. Sin. Technol.* **2018**, *48*, 691–700. [CrossRef]
12. Brohi, I.; Pooladi-Darvish, M.; Aguilera, R. Modeling Fractured Horizontal Wells As Dual Porosity Composite Reservoirs—Application to Tight Gas, Shale Gas and Tight Oil Cases. In Proceedings of the SPE Western North American Region Meeting, Anchorage, AK, USA, 7–11 May 2011. [CrossRef]
13. Wattenbarger, R.; El-Banbi, A.; Villegas, M.; Maggard, J.B. Production Analysis of Linear Flow into Fractured Tight Gas Wells. In Proceedings of the SPE Rocky Mountain Regional/Low-Permeability Reservoirs Symposium, Denver, CO, USA, 5–8 April 1998.

14. Alahmadi, H.A.H.; Wattenbarger, R.A. Triple-Porosity Models: One Further Step towards Capturing Fractured Reservoirs Heterogeneity. In Proceedings of the SPE/DGS Saudi Arabia Section Technical Symposium and Exhibition, Al-Khobar, Saudi Arabia, 15–18 May 2011.
15. Tivayanonda, V.; Apiwathanasorn, S.; Economides, C.; Wattenbarger, R.A. Alternative Interpretations of Shale Gas/Oil Rate Behavior Using a Triple Porosity Model. In Proceedings of the SPE Annual Technical Conference and Exhibition, San Antonio, TX, USA, 8–10 October 2012.
16. Xu, B.X.; Haghighi, M.; Cooke, D.; Li, X. Development of New Type Curves for Production Analysis in Naturally Fractured Shale Gas/Tight Gas Reservoirs. *J. Pet. Sci. Eng.* **2013**, *105*, 107–115. [CrossRef]
17. Stalgorova, K.; Mattar, L. Analytical Model for Unconventional Multifractured Composite Systems. *SPE Res. Eval. Eng.* **2013**, *16*, 246–256. [CrossRef]
18. Gringarten, A.C.; Ramey, H.J.; Raghavan, R. Unsteady-State Pressure Distribution Created by a Well With a Single Infinite-Conductivity Vertical Fracture. *SPE J.* **1972**, *14*, 347–360. [CrossRef]
19. Ozkan, E.; Raghavan, R. New Solutions for Well-Test Analysis Problems. Part 1: Analytical Considerations. *SPE Form. Eval.* **1991**, *6*, 359–368. [CrossRef]
20. Amini, S.; Valkó, P.P. Using Distributed Volumetric Sources to Predict Production from Multiple-Fractured Horizontal Wells under Non-Darcy-Flow Conditions. *SPE J.* **2010**, *15*, 105–115. [CrossRef]
21. Yang, D.; Zhang, F.; Styles, J.A.; Gao, J. Performance Evaluation of a Horizontal Well with Multiple Fractures by Use of a Slab-Source Function. *SPE J.* **2015**, *20*, 652–662. [CrossRef]
22. Kim, J.G.; Deo, M.D. Finite-Element, Discrete-Fracture Model for Multiphase Flow in Porous Media. *AIChE J.* **2000**, *46*, 1120–1130. [CrossRef]
23. Juanes, R.; Samper, J.; Molinero, J. A General and Efficient Formulation of Fractures and Boundary Conditions in the Finite Element Method. *Int. J. Numer. Methods Eng.* **2002**, *54*, 1751–1774. [CrossRef]
24. Bogdanov, I.I.; Mourzenko, V.V.; Thovert, J.-F.; Adler, P.M. Effective Permeability of Fractured Porous Media in Steady State Flow. *Water Resour. Res.* **2003**, *39*, 1023–1038. [CrossRef]
25. Zhang, R.H.; Zhang, L.H.; Wang, R.H.; Zhao, Y.L.; Zhang, D.L. Research on Transient Flow Theory of a Multiple Fractured Horizontal Well in a Composite Shale Gas Reservoir Based on the Finite-Element Method. *J. Nat. Gas Sci. Eng.* **2016**, *33*, 587–598. [CrossRef]
26. Pecher, R.; Harris, S.D.; Knipe, R.J.; Elliott, L.; Ingham, D.B. New Formulation of the Green Element Method to Maintain Its Second-Order Accuracy in 2d/3d. *Eng. Anal. Bound. Elem.* **2001**, *25*, 211–219. [CrossRef]
27. Taigbenu, A.E. *The Green Element Method*; Springer: New York, NY, USA, 1999.
28. Wang, Y.H.; Liang, J.P.; Zhang, J.Y.; Zhao, B.; Zhao, Y.; Liu, X.; Xia, D. Resource Potential and Exploration Direction of GuLong Shale Oil in Songliao Basin. *Pet. Geol. Oilfield Dev. Daqing* **2020**, *39*, 20–34.
29. Ding, M.; Jin, Z.; Zhang, Y.; Hu, J. A new mixed type crack propagation criterion in shale reservoirs. *Petroleum* **2024**, *10*, 85–92. [CrossRef]
30. Yang, H.; Yue, P.; Wang, Z.; Xiong, Y.; Fan, W.; Zhang, S.; Shi, W. Nanoscale flow model modelling and analysis of tight reservoir based on viscosity change and interfacial slip characteristics in confined space. *Petroleum* **2025**, *11*, 504–515. [CrossRef]

Disclaimer/Publisher's Note: The statements, opinions and data contained in all publications are solely those of the individual author(s) and contributor(s) and not of MDPI and/or the editor(s). MDPI and/or the editor(s) disclaim responsibility for any injury to people or property resulting from any ideas, methods, instructions or products referred to in the content.